

Quantum Phase Transitions of Interlayer Excitons in van der Waals Heterostructures

Jia-Pei Deng, Zi-Wu Wang,* Yu Cui, Yi-Yan Liu, Xin-Jun Ma,* Shao-Juan Li, and Zhi-Qing Li

Quantum phases of interlayer excitons (IXs) in van der Waals heterostructures (vdWHs) play a critical role in determining the fundamental properties of these structures. However, quantum phase transitions between free state and self-trapped state of IXs remain poorly understood. Herein, the physical pictures for quantum transitions of IXs stemming from the IX–interface optical phonon coupling are explored. The critical boundaries of the phase transitions among free, light, and heavy self-trapped states are given and the dependence of boundaries on the structural parameters of vdWHs is discussed, implying the controllability of these IXs states in vdWHs. In order to distinguish different quantum phases further, a strategy that multiphonon Raman scattering mediated by these exciton states is proposed. It is found that multiphonon overtones appear in Raman spectra for the self-trapped states and not for free states, which clarifies the long-standing puzzle that free exciton can induce multiphonon Raman processes. The results lay the significant theoretical foundation for understanding the quantum phases of IX and their modulation in vdWHs.

1. Introduction

Atomically thin 2D materials have created a revolution in materials science^[1–3] since the first isolation of graphene.^[4] The emergence of each new 2D material brings excitement and puzzles stemming from their electronic band structures and the resulting fascinating physical properties,^[1–3,5] which are substantially

different from those of their 3D counterparts. Furthermore, 2D materials can be held together by the weak van der Waals force, resulting in the so-called van der Waals heterostructures (vdWHs).^[3,6,7] As a new type of 2D structure, vdWHs not only combine the extraordinary properties of the constituent monolayers, but also provide a wide platform for exploring new fascinating physics.^[3,6–8] One novel physical phenomenon is the emergence of interlayer exciton (IX), i.e., spatially separated but bound electron–hole pair, which has been extensively predicted by theoretical studies^[9–11] and demonstrated by a series of experiments.^[12–15] The spatially indirect nature for IX reduces the overlap of the electron and hole wavefunctions, which results in its longer lifetime than the usual exciton (or intralayer exciton), reaching hundreds of nanoseconds^[12–14] or even


microseconds,^[15] and creates a permanent electrical dipole moment in the out-of-plane direction, allowing electrical control of its optical and transport properties.^[16–18] Compared with that in III–V or II–VI semiconductor heterostructures, this new type of exciton has remarkably high binding energy and is better stability. On the other hand, the interaction between IX and its phononic environment would become significant owing to a reduced screening effect in vdWHs, leading to the emergence of different quantum states of IX.

In general, the formation of self-trapped exciton could be attributed to the transient distorted lattice around it due to the strong exciton–phonon coupling, governing the optical and energy transport properties of vdWHs. Especially, in recent years, the efficient white photoluminescence emission in these vdWHs originating from the radiative recombination of the self-trapped excitons,^[19–21] promises a bright future in optoelectronic applications such as display and single-component light-emitting devices, and thus stimulates once again extensive studies of the self-trapped state. These studies have revealed that, compared with the free excitons, the self-trapped excitons can decay radiatively, yielding a distinctive luminescence, or nonradiatively, transferring energy to impurities, or forming lattice defects.^[20,22] Therefore, a fully understanding of the quantum transitions between the free state (FS) and the self-trapped state is of great importance for the design of high-performance vdWHs devices. Usually, FS and the self-trapped state are separated by an adiabatic potential barrier due to the exciton–phonon coupling,^[23–25]

J.-P. Deng, Z.-W. Wang, Y. Cui, Y.-Y. Liu, Z.-Q. Li
 Tianjin Key Laboratory of Dimensional Materials Physics and Preparing Technology
 Department of Physics
 School of Science
 Tianjin University
 Tianjin 300354, China
 E-mail: wangziwu@tju.edu.cn

X.-J. Ma
 College of Mathematics and Physics
 Inner Mongolia Minzu University
 Inner Mongolia, Tongliao 028043, China
 E-mail: xinjun@imn.edu.cn

S.-J. Li
 State Key Laboratory of Luminescence and Applications
 Changchun Institute of Optics
 Fine Mechanics and Physics Chinese Academy of Sciences
 Changchun 130033, China

 The ORCID identification number(s) for the author(s) of this article can be found under <https://doi.org/10.1002/pssr.202300242>.

DOI: 10.1002/pssr.202300242

implying exciton undergoes a transition between them with a change in the coupling strength. For these vdWHs, a large number of recent experiments^[26–29] have displayed phase transitions of excitons by some external conditions, such as the twist angle^[26,27] and strain,^[28,29] which inherently drive the exciton–phonon coupling strength required for the formation of the self-trapped state. In our previous work,^[30] we have investigated self-trapped IXs in vdWHs due to the strong IX–interface optical phonons coupling, where self-trapped IXs could be classified into heavy self-trapped (HST) state with the increasing binding energy and light self-trapped (LST) state with the decreasing binding energy. Nevertheless, the comprehensive picture of the quantum transitions and the critical boundaries among FS, LST, and HST for IXs remain lacking until now.

In this article, we systematically study the quantum phase transitions of IXs for an extensively used vdWHs (see **Figure 1a**), in which the self-trapped IXs are formed due to the strong IX–interface optical phonon coupling. We present phase diagrams of an IX based on a judging criterion of the self-trapped state—the self-energy $\Delta E_s > 0$, where they are specifically classified as LST and HST by means of the total binding energy correction $\Delta E_b > 0$ and < 0 , respectively. We find that the critical boundaries of the phase transitions among FS, LST, and HST undergo the significant shifts by the modulation of the structural distances and components of vdWHs. Furthermore, we propose multiphonon Raman scattering (MRS) mediated by three types of exciton states, respectively. It is found that high-order Raman peaks appear only for the self-trapped state and not for FS. This strategy provides a theoretical foundation to distinguish different exciton states and the phase transitions by Raman technology in future experiments.

Varieties of vdWHs are essentially endless with the continuous growth of the family of 2D materials, arising from the fact that they can be stacked in ambient conditions with no requirements of lattice matching, for example, the CHBS-type heterostructure (see **Figure 1a**: C—covering layer, HB—hosting bilayer for electron–hole pair, S—substrate layer). This is a classical structure widely used in the experimental and theoretical studies for IXs^[6,7,27] because the encapsulation of the structure is favorable for blocking the erosion of the internal 2D material by the external environment. Here, we mainly study the self-trapped properties of IXs in such a heterostructure.

2. Phase Transitions of IXs

For the CHBS-type heterostructure, the total Hamiltonian for IX coupling with interface optical phonons can be written as

$$H = H_{\text{ex}}^{\text{R}} + H_{\text{ex}}^{\text{T}} + H_{\text{ph}} + H_{\text{ex-ph}} \quad (1)$$

where $H_{\text{ex}}^{\text{R}} = -\hbar^2 \nabla_{\text{R}}^2 / (2M)$ and $H_{\text{ex}}^{\text{T}} = -\hbar^2 \nabla_{\text{r}}^2 / (2\mu) + V(r)$ are the center-of-mass motion and the relative motion of IX, respectively. $V(r)$ is the Coulomb interaction between electron and hole; $M = m_e + m_h$ and $\mu = (m_e^{-1} + m_h^{-1})^{-1}$ are the total mass and the reduced mass of IX. $H_{\text{ph}} = \sum_{\mathbf{q}} \hbar \omega_{\mathbf{q}} a_{\mathbf{q}}^{\dagger} a_{\mathbf{q}}$ denotes the interface optical phonon term, where $a_{\mathbf{q}}$ ($a_{\mathbf{q}}^{\dagger}$) is annihilation (creation) operator of a phonon with wave vector \mathbf{q} and $\hbar \omega_{\mathbf{q}}$ is the effective phonon energy, depending on the transverse and longitudinal

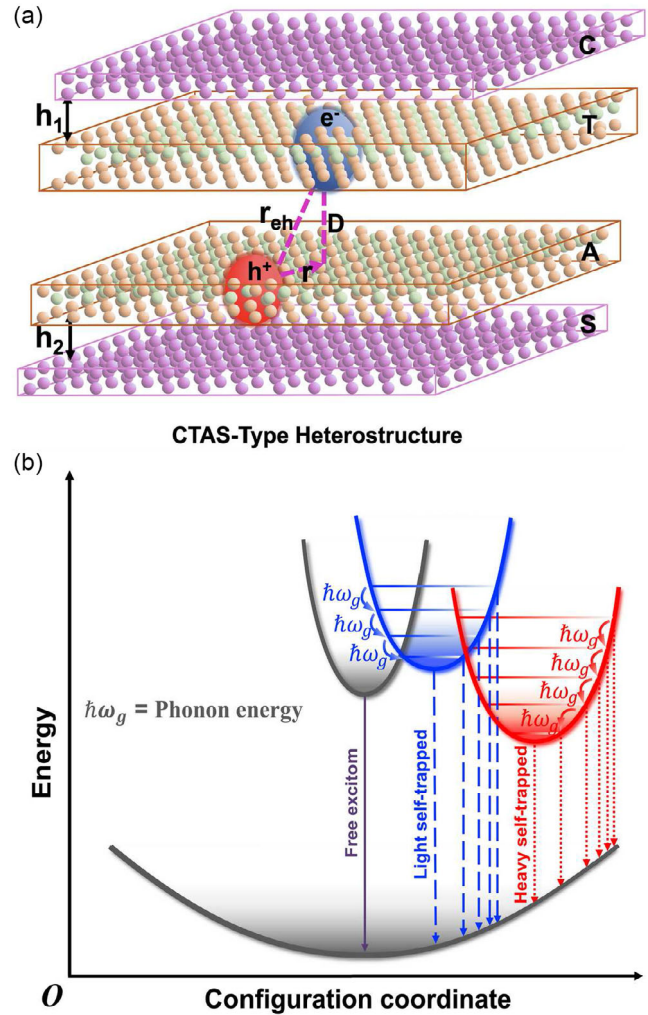


Figure 1. a) The schematic diagram of the IX in CHBS-type heterostructure (C—covering layer, HB—hosting bilayer for electron–hole pair, S—Substrate layer), where D is the vertical distance between HB, r_{eh} and r are the spatial and relative distances for the electron–hole pair, respectively. In such heterostructure, HB can be chosen in the huge members of 2D materials family; meanwhile, the covering and substrate materials also have manifold selections, resulting in the various dielectric environment for IXs and the different phonon modes couple with them. b) The schematic diagrams of FS, LST, and HST states of exciton.

optical (LO) phonon modes of the layer materials of vdWHs (see Equation (S7) and (S8), Supporting Information) based on the dielectric continuum model,^[30] which is reformulated via $\hbar \omega_{\mathbf{q}} = \hbar^2 q_0^2 / (2M)$,^[31–34] where $q_0 = \sqrt{2M\omega_g / \hbar}$ is defined as a variational quantity in following sections, just qualitatively reflecting the diversity of components of vdWHs because both M and ω_g vary with components. The last term $H_{\text{ex-ph}}$ represents the exciton–phonon coupling and is expressed as

$$H_{\text{ex-ph}} = \sum_{\mathbf{q}} \left\{ e^{i\mathbf{q}\cdot\mathbf{R}} [\mathcal{M}_h e^{-i\gamma_1 \mathbf{q}\cdot\mathbf{r}} - \mathcal{M}_e e^{i\gamma_2 \mathbf{q}\cdot\mathbf{r}}] a_{\mathbf{q}} + e^{-i\mathbf{q}\cdot\mathbf{R}} [\mathcal{M}_h e^{i\gamma_1 \mathbf{q}\cdot\mathbf{r}} - \mathcal{M}_e e^{-i\gamma_2 \mathbf{q}\cdot\mathbf{r}}] a_{\mathbf{q}}^{\dagger} \right\} \quad (2)$$

where $\gamma_1 = m_e/M$, $\gamma_2 = m_h/M$; $\mathcal{M}_{e(h)} = [\nu_{e(h)}e_*^2 / (\epsilon q L^2)]^{1/2} e^{-qz}$ is the coupling element between electron (hole) and interface optical phonons given by the dielectric continuum model,^[30] in which ν_h and ν_e are the parameters of hosting dielectric environment for hole and electron (Equation (S6) and (S5), Supporting Information), respectively; e_* is the charge of carrier, ϵ is vacuum dielectric constant, L^2 is the quantization area in the monolayer plane, and z represents the interlayer spacing, such as h_1 and h_2 in Figure 1a, denoting the distance between hosting layer and covering layer and substrate layer, respectively.

Carrying out the Lee–Low–Pines unitary transformation^[35] for the total Hamiltonian in Equation (1) (see Section SI, Supporting Information, for details), the transformed Hamiltonian is rewritten as

$$\begin{aligned} \tilde{H} = & \frac{\hbar^2 Q^2}{2M} - \frac{\hbar^2}{2\mu} \nabla_{\mathbf{r}}^2 + V(\mathbf{r}) + \sum_{\mathbf{q}} \left(\frac{\hbar^2 \mathbf{q}^2}{2M} + \hbar\omega_{\mathbf{g}} \right) a_{\mathbf{q}}^\dagger a_{\mathbf{q}} \\ & - \sum_{\mathbf{q}} \frac{|\mathcal{M}_h|^2 + |\mathcal{M}_e|^2 - \mathcal{M}_h^* \mathcal{M}_e \Xi_{\mathbf{q}}(\mathbf{r})}{\hbar^2 \mathbf{q}^2 / (2M) + \hbar\omega_{\mathbf{g}}} \\ & + \sum_{\mathbf{q}} \frac{\hbar^2 \mathbf{q}^2}{2\mu} \frac{1}{[\hbar^2 \mathbf{q}^2 / (2M) + \hbar\omega_{\mathbf{g}}]^2} \\ & \times [\gamma_1^2 |\mathcal{M}_h|^2 + \gamma_2^2 |\mathcal{M}_e|^2 + \gamma_1 \gamma_2 \mathcal{M}_h^* \mathcal{M}_e \Xi_{\mathbf{q}}(\mathbf{r})] \end{aligned} \quad (3)$$

with

$$\Xi_{\mathbf{q}}(\mathbf{r}) = \exp[-i(\gamma_1 + \gamma_2)\mathbf{q} \cdot \mathbf{r}] + \exp[i(\gamma_1 + \gamma_2)\mathbf{q} \cdot \mathbf{r}] \quad (4)$$

where one phonon term and the interactions between different phonons for the center-of-mass motion and the relative motion are neglected in Equation (3) due to the tiny contribution to the binding energy. Meanwhile, we assume the center-of-mass is frozen in the ground state ($Q = 0$) because it is not related to the exciton binding energy.

The total correction of exciton binding energy ΔE_b can be obtained via $\langle \Phi | \tilde{H} | \Phi \rangle$, where the system wave function $|\Phi\rangle = |\varphi_{1s}\rangle |0\rangle_{\text{ph}}$ is the product of the zero-phonon state $|0\rangle_{\text{ph}}$ and the ground state of the relative motion $|\varphi_{1s}\rangle$. The latter is given by $|\varphi_{1s}\rangle = \sqrt{\beta/\pi} \exp(-\beta \mathbf{r}^2/2)$ in the harmonic oscillator approximation,^[36,37] with the variational parameter β , depending on the vertical distance between the hosting layers of electron and hole (Equation (S3), Supporting Information). After the complicated calculation, one can find that ΔE_b could be attributed to the Coulomb potential correction ΔE_c and the self-energy ΔE_s , satisfying the relation of $\Delta E_b = \Delta E_s - \Delta E_c$. ΔE_c and ΔE_s can be written as

$$\begin{aligned} \Delta E_c = & \sum_{\mathbf{q}} \alpha \nu_e e^{-2q h_1} \left[\frac{2q_0}{q^2 + q_0^2} \xi^{\frac{1}{2}} e^{-q(\eta-1)h_1} \right. \\ & \left. + \frac{2q_0 q^2}{(q^2 + q_0^2)^2} \xi^{\frac{1}{2}} e^{-q(\eta-1)h_1} \right] \Omega(\mathbf{q}) \end{aligned} \quad (5)$$

$$\begin{aligned} \Delta E_s = & \sum_{\mathbf{q}} \alpha \nu_e e^{-2q h_1} \left[\frac{q_0}{q^2 + q_0^2} (\xi e^{-2q(\eta-1)h_1} + 1) \right. \\ & \left. - \frac{q_0 q^2}{(q^2 + q_0^2)^2} (\sigma \xi e^{-2q(\eta-1)h_1} + \frac{1}{\sigma}) \right] \end{aligned} \quad (6)$$

where $\Omega(\mathbf{q}) = \exp[-\mathbf{q}^2 / (4\beta)]$, α represents a dimensionless constant for the IX–interface optical phonon coupling (Equation (S17), Supporting Information), which determines the magnitude of ΔE_s and ΔE_b ; the ratio parameter $\xi = \nu_h/\nu_e$ is called as

the dielectric factor, describing the asymmetry of the dielectric environment surrounding electrons and holes arising from the different componential material of vdWHs, such as the various choices for the hosting layer of holes (electrons) and substrate (covering) layer; the ratio parameter $\eta = h_2/h_1$ describes the structural asymmetry of vdWHs, resulting from the asymmetrical variation of internal distances for h_2 and h_1 ; $\sigma = m_e/m_h$ is the ratio of the electron-to-hole effective mass. These three ratio parameters play the central roles to modulate the quantum phases of IXs in vdWHs.

To obtain the phase diagram of IXs, the key prerequisite is how to judge the formations of self-trapped exciton states. Here, the self-energy $\Delta E_s > 0$ is used as a judging criterion following the previous studies.^[30,31,38,39] Based on this criterion, the total correction of binding energy could be specified into $\Delta E_b > 0$ and < 0 , which are called as HST and LST, respectively. Therefore, the phase diagrams of IXs are composed of FS, HST, and LST in this article. In addition, IXs include two species according to the spin selection rules and the spin–orbital interaction between the valence and conduction bands in vdWHs. We assume they have the similar behaviors.

According to the judging criterion above mentioned, the different regions for FS, LST, and HST in the σ – q_0 plane are shown in Figure 2a,c. The phase transitions among three types of IX states follow several different paths under the interplays between σ and q_0 at different η and ξ . From them, one can conclude that the phase transition from the FS to HST occurred hardly unless with the help of a mediated state LST, which is consistent with earlier studies that the exciton ground state changes discontinuously between the FS and HSTs with a change in the exciton–lattice coupling constant.^[40–43] However, the LST of exciton has yet been pointed out until our recent work,^[30] because of the challenging identification of the LST in practice that its smaller binding energy than FS, confusing with the excited states of free exciton. Although some traces that the blueshift and broadened linewidth in the IX spectra at low temperature have been found in recent experiment,^[44] more experimental verifications for this LST are urgent.

Another remarkable feature is that the critical boundaries of the phase transitions undergo a shift by tuning η and ξ . First, let us discuss the detailed variation of the critical boundaries at different η (h_2/h_1) shown in Figure 2b. When q_0 is in the region of small values ($0.1 \approx 1$), there only exist the phase transitions between the FS and LST. The region of FS expands and contracts for the mass ratio σ (m_e/m_h) < 0.23 and > 3.9 , respectively, with increasing η , which can be attributed to the asymmetrical contribution of hole and electron to the self-energy term, originally causing by the different influence between h_1 and h_2 on the electron and hole–interface optical phonon coupling as given in Equation (S4) and S(5), Supporting Information, respectively. Generally, this region may be the ideal realm for the identify of LST without the appearance of HST. With increasing q_0 , the phase transitions are occurred between the LST and HST. The variation of them can be divided into three regions: the first region for $\sigma > 2$, HST gradually expands as η increases; the second region for $0.6 < \sigma < 2$, HST contracts at $\eta < 1$ and expanded at $\eta > 1$; and the third region for $\sigma < 0.6$, HST is also a contraction followed by an expansion, whereas the turning point between contraction and expansion differs from the second

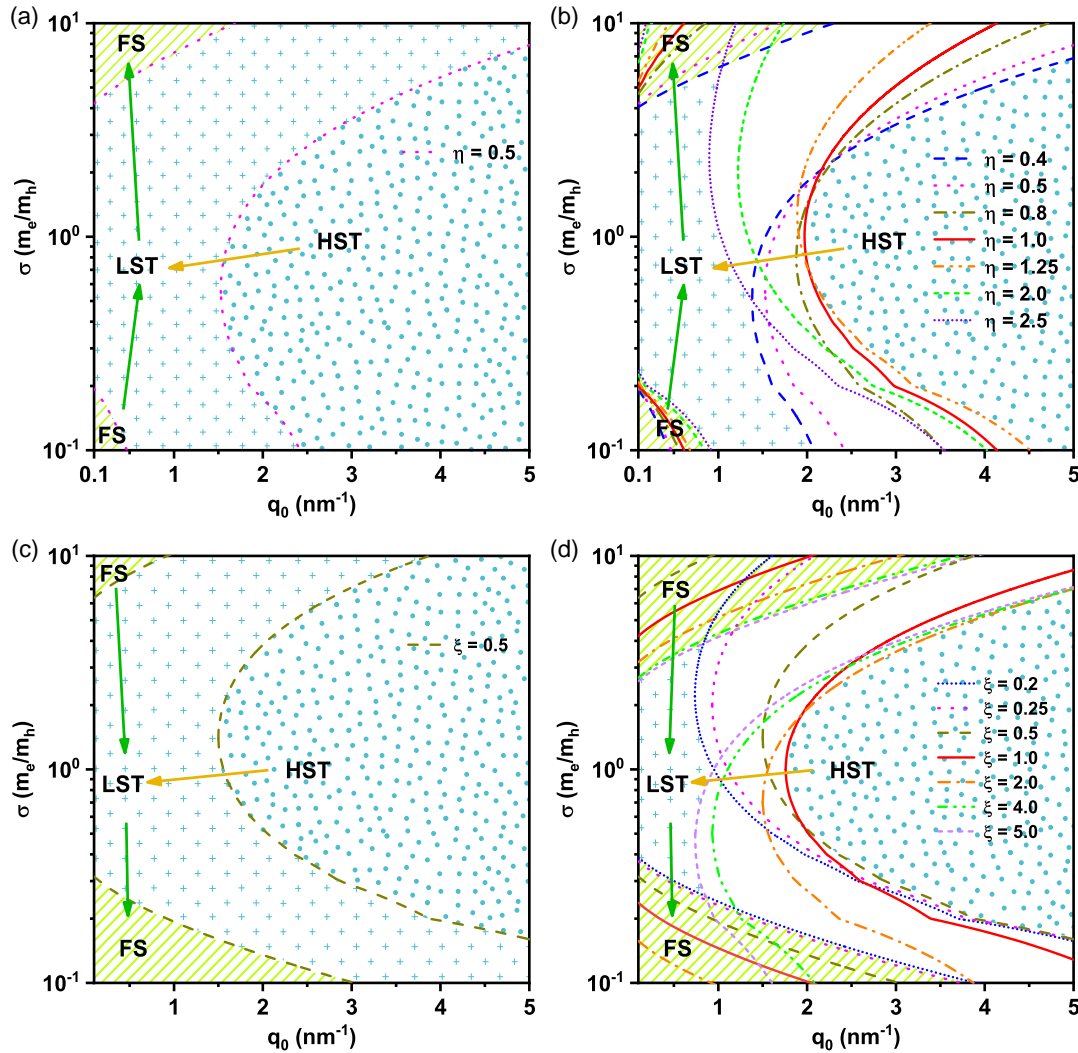


Figure 2. The phase diagrams of IXs. a) The phase diagrams of the FS, HST state, and LST state in the σ - q_0 plane at $\eta = 0.5$. b) The variation of the boundaries of quantum phases for different η at $\beta = 0.6 \text{ nm}^{-2}$, $h_1 = 1.0 \text{ nm}$, and $\nu_h = \nu_e$. c) The phase diagrams of the FS, HST state, and LST state in the σ - q_0 plane at $\xi = 0.5$. d) The variation of the boundaries of quantum phases for different ξ at $\beta = 0.6 \text{ nm}^{-2}$, $\nu_e = 0.4 \text{ meV}$, and $h_1 = h_2 = 0.3 \text{ nm}$.

region. These complicated phase transitions between the LST and HST could be tuned by η , implying that the significant influence of the stacking distances between the covering (substrate) layer and hosting layer for holes (electrons) on the fundamental properties of IXs, both of which may be reflected by the variation of the linewidth in the spectra of self-trapped IXs.^[44,45] The dielectric environment that composed of the hosting layer and the covering layer (substrate layer) for the electrons (holes) is described by the parameter ν_e (ν_h) given in Equation (S5) and (S6), Supporting Information, which could be varied in the wide range due to various of collocations among 2D materials family. The influence of the dielectric factor ξ (ν_h/ν_e) on the phase transitions in the σ - q_0 plane at fixed $\eta = 1$ is shown in Figure 2d. It is obvious that 1) the dependence of phase diagrams on q_0 follows the similar trends presented in Figure 2b except for the slightly expansion of FS's region; 2) the region of HST is expanded obviously for $\xi > 1$ or $\xi < 1$, which implies that these HSTs of IX are more easily obtained when hole and electron are in unequal

hosting environment; and 3) the critical boundaries between LST and HST show the symmetrical shifting with respect to the varying from $\xi = 1$ to $\xi = 5$ and from $\xi = 1$ to $\xi = 0.2$ due to the exchange effect. For example, for the cases of $\xi = 2$ and $\xi = 0.5$, meaning the exchange of the hosting dielectric environment for electrons with holes. In fact, just this exchange effect results in the expansion and contraction of the region of FS for $\sigma < 1$ or $\sigma > 1$ with increasing ξ , respectively. In addition, we investigate the effect of the spatial distance D between electron and hole on the phase transitions (Figure S1, Supporting Information). One can find that the changing of this distance has no influence on the phase transitions between the FS and LST. But the region of HST is expanded remarkably with increasing D , so the stability of these excitons will become fragile, which is consistent with our previous work.^[30] Besides the general ways related to three ratio parameters abovementioned for the modulation of IXs, the moiré angle between two hosting layers, such as heterostructures based on monolayer transition metal

dichalcogenides and graphene,^[46,47] could enhance the self-trapped effect due to the strong quantum confinement of the moiré potential, which further enriches the controllable ways for the modulation of IXs in vdWHs. In addition, transitions among three phases of IX, in fact, are temperature dependences. This is just the reason why the variations of exciton states are called as quantum phase transitions. The studies for the temperature dependences of excitonic phases will be presented in the future work.

3. Raman Scattering Mediated by IXs

In order to identify these phase transitions of IXs in vdWHs, we propose a theoretical strategy that Raman scattering mediated by these IXs states. We hope the symbolic features of different quantum phases of IXS could be directly reflected by Raman spectra. In the frame of Huang–Rhys model,^[48,49] the cross section of Raman scattering at finite temperature is given by (see Section SII, Supporting Information for the detailed derivations)

$$|\mathcal{R}_p|^2 = \mu_e^4 \left| \frac{\prod_g \left(\frac{\bar{n}_g + 1}{\bar{n}_g} \right)^{\frac{p}{2}} e^{-S_g(2\bar{n}_g + 1)} I_p \left\{ 2S_g \sqrt{\bar{n}_g(\bar{n}_g + 1)} \right\}}{E_{el} + p\hbar\omega_g - \hbar\omega_i + i\Gamma} \right|^2 \quad (7)$$

where μ_e is the electronic transition dipole moment; $\bar{n}_g = 1/(e^{\hbar\omega_g/K_B T} - 1)$ denotes the thermal average of the phonon number (T is temperature and K_B is the Boltzmann constant); I_p is the p th-order modified Bessel function ($p = 1, 2, 3 \dots$); E_{el} is the needed energy for the creation of an IX in the ground state; $\hbar\omega_i$ is the incident photon energy; and Γ is the homogeneous linewidth of excitonic state. S_g is the Huang–Rhys factor and plays a key role in determining multiphonon processes. This factor can be calculated by

$$S_g^{FS} = \sum_q \left(\frac{1}{\hbar\omega_g} \right)^2 \left| \left(\frac{\nu_h \epsilon^2}{\epsilon q L^2} \right)^{\frac{1}{2}} e^{-q h_2} e^{-\frac{q^2}{4\beta_h}} - \left(\frac{\nu_e \epsilon^2}{\epsilon q L^2} \right)^{\frac{1}{2}} e^{-q h_1} e^{-\frac{q^2}{4\beta_e}} \right|^2 \quad (8)$$

for the free exciton state and

$$S_g^{LST(HST)} = \sum_q \left(\frac{1}{\hbar\omega_g} \right)^2 \left| \left(\frac{\nu_h \epsilon^2}{\epsilon q L^2} \right)^{\frac{1}{2}} e^{-q h_2} e^{-\frac{q^2}{4\beta_h}} + \left(\frac{\nu_e \epsilon^2}{\epsilon q L^2} \right)^{\frac{1}{2}} e^{-q h_1} e^{-\frac{q^2}{4\beta_e}} \right|^2 \quad (9)$$

for the light or HST states, where $\beta_e = 1/(2a_e^2)$ and $\beta_h = 1/(2a_h^2)$ with $a_e = \sqrt{\hbar/(2m_e\omega_g)}$ and $a_h = \sqrt{\hbar/(2m_h\omega_g)}$ are the radii of the electron polaron and hole polaron, respectively. Here, we select the structure of $\text{Al}_2\text{O}_3/\text{MAPbI}_3/(\text{PEA})_2\text{PbI}_4/\text{Al}_2\text{O}_3$ as an example to show the features of Raman spectra for these IXs states, as shown in **Figure 3**, where MAPbI_3 and $(\text{PEA})_2\text{PbI}_4$ are two typical 2D metal halide perovskites materials and the related parameters are listed in Table S1, Supporting Information. Figure 3a shows Raman scattering of IXs with increasing the dielectric factor ξ (ν_h/ν_e). According to the dependences of phase transitions of IXs on ξ given in Figure 2d, one can see that multiple phonons Raman scattering occurred for both LST and HST, not for FS. Moreover, the phase transitions from FS to LST as well as from LST to HST at certain values of ξ could be reflected directly in Raman spectra, which is an agreement with the prediction in Figure 2d. Meanwhile, orders of phonon overtones increase gradually from LST to HST, where the strongest overtone shows the blueshifting behavior. Both of them display the discrepancies of the lattice relaxation effect between LST and HST, which also could be evaluated quantitatively by the well-known Huang–Rhys factors given in Table S2, Supporting Information. In fact, self-trapped exciton states arising from the strong coupling between the excitons and phonons lead to a number of phonon replicas, which have been observed in many optical experiments, such as the LO phonon replicas of free excitons and neutral donor-bound excitons,^[50–52]

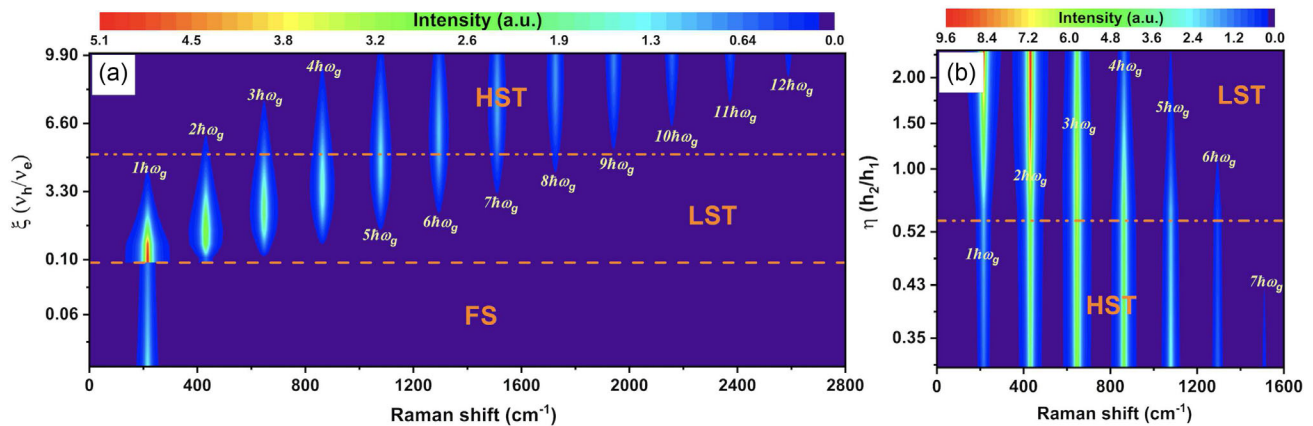


Figure 3. a) Raman scattering mediated by FS, LST, and HST of IXs for different ξ at temperature $T = 77$ K, $M = 0.85 m_0$, $\hbar\omega_g = 26.81$ eV, $\nu_e = 0.3$ meV, $\sigma = 0.29$, $\beta = 0.6$ nm⁻², and $h_1 = h_2 = 0.3$ nm, where m_0 is the electronic static mass. The dashed lines show the boundaries between FS and LST as well as LST and HST. b) Raman scattering mediated by LST and HST of IXs for different η at $M = 0.85 m_0$, $\hbar\omega_g = 26.81$ eV, $h_1 = 1.0$ nm, $\sigma = 0.29$, $\beta = 0.6$ nm⁻², $\nu_h = 0.35$ meV, and $\nu_e = 1.0$ meV.

as well as MRS.^[53–58] In particular, the strength of exciton–phonon coupling, the lattice distortion, and the change in vibrational modes can be directly evaluated by MRS. However, what puzzle is that MRS can also be induced by FS in many past experiments.^[50,51,59–63] Although some researchers have attributed it to hot exciton effect, the existence of strong exciton–phonon coupling and the rapid decay of the intensity of multiphonon peaks render this explanation lacking in credibility. From Figure 3a, it can be concluded that 1) FS cannot induce MRS; and 2) LST with smaller binding energy than FS, but stronger lattice relaxation, could provide a better explanation for these experimental measurements than the mechanism of hot exciton states.

The modulation of the ratio parameter η (h_2/h_1) on Raman scattering of IXs is shown in Figure 3b, where only the phase transition from LST to HST and the corresponding multiphonon scattering with the similar trends in Figure 3a are shown, but not for the FS of exciton, which can be attributed to the insensitively modulation of the phase of FS by the parameter η shown in Figure 2b. In addition, the number of phonon overtones for LST and HST has far less orders than those in Figure 3a because the Huang–Rhys factors under this condition (shown in Table S3, Supporting Information) are much smaller than those in Table S2, Supporting Information, which implies that the material asymmetry for vdWHs, due to the versatile stacking combinations among the huge members of 2D material family, has much more significant effect on the strength of IX–interface optical phonon coupling than structural asymmetry.

4. Conclusion

In summary, we investigate the quantum phase transitions of IX in vdWHs stemming from the IX–interface optical phonons coupling. We find that 1) the critical boundaries of the phase transition among three types of IX states could be modulated by three key parameters of vdWHs: the mass ratio σ , the structural asymmetry parameter η , and the dielectric factor ξ , which implies the controllability of these exciton states; and 2) multiphonon overtones appear for the self-trapped states, not for FS of IXs, showing that MRS could be used to distinguish them, which also clarifies the long-standing question that the excited-state of free exciton (or hot exciton) could induce multiphonon Raman processes. Our results provide the significant foundation for analyzing the phase transitions of IXs from free to self-trapped states in various of vdWHs.

Supporting Information

Supporting Information is available from the Wiley Online Library or from the author.

Acknowledgements

This work was supported by the National Natural Science Foundation of China (grant nos. 12174283, 12164032, 62022081, and 61974099).

Conflict of Interest

The authors declare no conflict of interest.

Data Availability Statement

The data that support the findings of this study are available from the corresponding author upon reasonable request.

Keywords

free states, interlayer excitons, phase transitions, self-trapped states, van der Waals heterostructures

Received: July 2, 2023

Revised: September 28, 2023

Published online: October 17, 2023

- [1] P. Ares, K. S. Novoselov, *Nano Mater. Sci.* **2022**, *4*, 3.
- [2] K. S. Novoselov, D. Jiang, F. Schedin, T. J. Booth, V. V. Khotkevich, S. V. Morozov, A. K. Geim, *Proc. Natl. Acad. Sci. U.S.A.* **2005**, *102*, 10451.
- [3] K. S. Novoselov, A. Mishchenko, A. Carvalho, A. H. Castro Neto, *Science* **2016**, *353*, aac9439.
- [4] K. S. Novoselov, A. K. Geim, S. V. Morozov, D. E. Jiang, Y. S. Zhang, S. V. Dubonos, I. V. Grigorieva, A. A. Firsov, *Science* **2004**, *306*, 666.
- [5] F. Hüser, T. Olsen, K. S. Thygesen, *Phys. Rev. B* **2013**, *87*, 235132.
- [6] A. K. Geim, I. V. Grigorieva, *Nature* **2013**, *499*, 419.
- [7] Y. Liu, N. O. Weiss, X. D. Duan, H. C. Cheng, Y. Huang, X. F. Duan, *Nat. Rev. Mater* **2016**, *1*, 16042.
- [8] E. V. Calman, C. J. Dorow, M. M. Fogler, L. V. Butov, S. Hu, A. Mishchenko, A. K. Geim, *Appl. Phys. Lett.* **2016**, *108*, 101901.
- [9] N. R. Wilson, P. V. Nguyen, K. Seyler, P. Rivera, A. J. Marsden, Z. P. L. Laker, G. C. Constantinescu, V. Kandyba, A. Barinov, N. D. M. Hine, X. D. Xu, D. H. Cobden, *Sci. Adv.* **2017**, *3*, 1601832.
- [10] E. Torun, H. P. C. Miranda, A. Molina-Sánchez, L. Wirtz, *Phys. Rev. B* **2018**, *97*, 245427.
- [11] T. Deilmann, K. S. Thygesen, *Nano Lett.* **2018**, *18*, 2984.
- [12] B. Miller, A. Steinhoff, B. Pano, J. Klein, F. Jahnke, A. Holleitner, U. Wurstbauer, *Nano Lett.* **2017**, *17*, 5229.
- [13] M. Baranowski, A. Surrente, L. Klopotoski, J. M. Urban, N. Zhang, D. K. Maude, K. Wiwatowski, S. Mackowski, Y. C. Kung, D. Dumcenco, A. Kis, P. Plochocka, *Nano Lett.* **2017**, *17*, 6360.
- [14] P. Nagler, M. V. Ballottin, A. A. Mitigloglu, F. Mooshammer, N. Paradiso, C. Strunk, R. Huber, A. Chernikov, P. C. M. Christianen, C. Schüller, T. Korn, *Nat. Commun.* **2017**, *8*, 1551.
- [15] C. Y. Jiang, W. G. Xu, A. Rasmita, Z. M. Huang, K. Li, Q. H. Xiong, W. B. Gao, *Nat. Commun.* **2018**, *9*, 753.
- [16] H.-P. Wang, S.-Y. Li, X.-Y. Liu, Z.-F. Shi, X.-S. Fang, J.-H. He, *Adv. Mater.* **2020**, *33*, 2003309.
- [17] L. A. Jauregui, A. Y. Joe, K. Pistunova, D. S. Wild, A. A. High, Y. Zhou, G. Scuri, K. De Greve, A. Sushko, C. H. Yu, T. Taniguchi, K. Watanabe, D. J. Needleman, M. D. Lukin, H. Park, P. Kim, *Science* **2019**, *366*, 870.
- [18] A. Ciarrocchi, D. Unuchek, A. Avsar, K. Watanabe, T. Taniguchi, A. Kis, *Nat. Photonics* **2019**, *13*, 131.
- [19] E. R. Dohner, A. Jaffe, L. R. Bradshaw, H. I. Karunadasa, *J. Am. Chem. Soc.* **2014**, *136*, 13154.
- [20] L. L. Mao, P. J. Guo, M. Kepenekian, I. Hadar, C. Katan, J. Even, R. D. Schaller, C. C. Stoumpos, M. G. Kanatzidis, *J. Am. Chem. Soc.* **2018**, *140*, 13078.

- [21] M. D. Smith, H. I. Karunadasa, *Acc. Chem. Res.* **2018**, *51*, 619.
- [22] X. M. Wang, W. W. Meng, W. Q. Liao, J. B. Wang, R. G. Xiong, Y. F. Yan, *J. Phys. Chem. Lett.* **2019**, *10*, 501.
- [23] K. S. Song, R. T. Williams, *Self-Trapped Excitons*, 2nd ed., Springer-Verlag Berlin Heidelberg, Berlin **1996**.
- [24] M. Ueta, H. Kanzaki, K. Kobayashi, Y. Toyozawa, E. Hanamura, *Excitonic Processes in Solids*, 1st ed., Springer-Verlag Berlin Heidelberg, Berlin **1986**.
- [25] A. Sumi, *J. Phys. Soc. Jpn.* **1977**, *43*, 1286.
- [26] K. L. Seyler, P. Rivera, H. Y. Yu, N. P. Wilson, E. L. Ray, D. G. Mandrus, J. Q. Yan, W. Yao, X. D. Xu, *Nature* **2019**, *567*, 66.
- [27] K. Tran, G. Moody, F. C. Wu, X. B. Lu, J. Choi, K. Kim, A. Rai, D. A. Sanchez, J. Quan, A. Singh, J. Embley, A. Zepeda, M. Campbell, T. Autry, T. Taniguchi, K. Watanabe, N. Lu, S. K. Banerjee, K. L. Silverman, S. Kim, E. Tutuc, L. Yang, A. H. MacDonald, X. Q. Li, *Nature* **2019**, *567*, 71.
- [28] Y. M. He, Y. Yang, Z. H. Zhang, Y. J. Gong, W. Zhou, Z. L. Hu, G. L. Ye, X. Zhang, E. Bianco, S. D. Lei, Z. H. Jin, X. L. Zou, Y. C. Yang, Y. Zhang, E. Q. Xie, J. Lou, B. Yakobson, R. Vajtai, B. Li, A. Pulickel, *Nano Lett.* **2016**, *16*, 3314.
- [29] W. Wang, X. D. Ma, *ACS Photonics* **2020**, *7*, 2460.
- [30] J. P. Deng, H. J. Li, X. F. Ma, X. Y. Liu, Y. Cui, X. J. Ma, Z. Q. Li, Z. W. Wang, *J. Phys. Chem. Lett.* **2020**, *13*, 3732.
- [31] S. W. Gu, M. Y. Shen, *Phys. Rev. B* **1987**, *35*, 9817.
- [32] Z. G. Yu, *J. Chem. Phys.* **2022**, *156*, 124706.
- [33] J. Q. Miao, Q. L. Yang, S. W. Gu, *Phys. Rev. B* **1989**, *40*, 9846.
- [34] W. S. Li, S. W. Gu, T. Au Yeung, Y. Y. Yeung, *Phys. Rev. B* **1992**, *46*, 4630.
- [35] T. D. Lee, F. E. Low, D. Pines, *Phys. Rev.* **1953**, *90*, 297.
- [36] O. L. Berman, G. Gumbs, R. Y. Kezerashvili, *Phys. Rev. B* **2017**, *96*, 014505.
- [37] O. L. Berman, R. Y. Kezerashvili, *Phys. Rev. B* **2017**, *96*, 094502.
- [38] B. H. Wei, X. J. Zhao, S. W. Gu, *Phys. Rev. B* **1990**, *41*, 1368.
- [39] B. H. Wei, S. W. Gu, *Phys. Rev. B* **1991**, *43*, 9190.
- [40] Y. Toyozawa, *Prog. Theor. Phys.* **1961**, *26*, 29.
- [41] E. Rashba, *Opt. Spektrosk.* **1957**, *2*, 75.
- [42] H. Sumi, Y. Toyozawa, *J. Phys. Soc. Jpn.* **1971**, *31*, 342.
- [43] K. Cho, Y. Toyozawa, *J. Phys. Soc. Jpn.* **1971**, *30*, 1555.
- [44] O. Karni, E. Barré, S. C. Lau, R. Gillen, E. Y. Ma, B. Kim, K. Watanabe, T. Taniguchi, J. Maultzsch, K. Barmak, R. H. Page, T. F. Heinz, *Phys. Rev. Lett.* **2019**, *123*, 247402.
- [45] R. Kumar, I. Verzhbitskiy, F. Giustiniano, T. P. Sidiropoulos, R. F. Oulton, G. Eda, *2D Mater.* **2018**, *5*, 041003.
- [46] M. Y. Liu, L. P. Wang, G. Yu, *Adv. Sci.* **2022**, *9*, 2103170.
- [47] D. Huang, J. Choi, C. K. Shih, X. Q. Li, *Nat. Nanotechnol.* **2022**, *17*, 227.
- [48] K. Huang, A. Rhys, *Proc. R. Soc. A* **1950**, *204*, 406.
- [49] K. Huang, *Selected Papers of Kun Huang*, World Scientific, Singapore **2000**.
- [50] A. Teke, Ü. Özgür, S. Doğan, X. Gu, H. Morkoç, B. Nemeth, J. Nause, H. O. Everitt, *Phys. Rev. B* **2004**, *70*, 195207.
- [51] Ü. Özgür, Y. I. Alivov, C. Liu, A. Teke, M. Reshchikov, S. Doğan, V. Avrutin, S. J. Cho, H. Morkoç, *J. Appl. Phys.* **2005**, *98*, 11.
- [52] Z. Hennighausen, J. Moon, K. M. McCreary, C. H. Li, O. M. van't Erve, B. T. Jonker, *ACS Nano* **2023**, *17*, 2529.
- [53] Z. W. Wang, Y. Xiao, J. P. Deng, Y. Cui, Z. Q. Li, *Phys. Rev. B* **2019**, *100*, 125308.
- [54] Z. W. Wang, J. P. Deng, Y. Xiao, Z. Q. Li, *Phys. Status Solidi RRL* **2020**, *14*, 1900517.
- [55] T. Suzuki, K. Tanimura, N. Itoh, *Phys. Rev. B* **1994**, *49*, 7233.
- [56] K. X. Xu, J. M. Lai, Y. F. Gao, F. L. Song, Y. J. Sun, P. H. Tan, J. Zhang, *Phys. Rev. B* **2022**, *106*, 085205.
- [57] J. Z. Li, J. C. Hu, J. Q. Ma, X. L. Wen, D. H. Li, *Chin. Opt. Lett.* **2021**, *19*, 103001.
- [58] K. X. Xu, Z. R. Zhou, J. Zhang, *J. Phys. Chem. Lett.* **2022**, *14*, 32.
- [59] Q. H. Tan, Y. J. Sun, X. L. Liu, Y. Y. Zhao, Q. H. Xiong, P. H. Tan, J. Zhang, *2D Mater.* **2017**, *4*, 031007.
- [60] C. Singh, S. Rath, *J. Appl. Phys.* **2013**, *113*, 163104.
- [61] W. C. Jin, H. H. Kim, Z. P. Ye, G. H. Ye, L. Rojas, X. P. Luo, B. W. Yang, F. Z. Yin, J. S. A. Horng, S. J. Tian, Y. Fu, G. J. Xu, H. Deng, H. C. Lei, A. W. Tsen, K. Sun, R. He, L. Y. Zhao, *Nat. Commun.* **2020**, *11*, 4780.
- [62] L. Qin, Z. L. Wen, X. X. Zhang, K. Zhang, Y. X. Lin, L. Song, X. J. Wu, X. H. Qiu, *J. Phys. Chem. Lett.* **2020**, *11*, 8483.
- [63] T. Livneh, J. E. Spanier, *2D Mater.* **2015**, *2*, 035003.